ATLAS NOTE

ATLAS-CONF-2012-154

November 11, 2012

Search for direct production of charginos and neutralinos in events with three leptons and missing transverse momentum in 13.0 fb^{-1} of pp collisions at $\sqrt{s} = 8$ TeV with the ATLAS detector

The ATLAS Collaboration

Abstract

A search for the direct production of charginos and neutralinos in final states with three leptons (electrons or muons) and missing transverse momentum is presented. The analysis uses 13.0 fb^{-1} of proton-proton collision data delivered by the LHC at $\sqrt{s} = 8$ TeV and recorded by the ATLAS detector. No excess above the Standard Model expectation is observed in three signal regions that are either enriched or depleted in Z-boson decays. Limits are placed at the 95% confidence level on the masses of the charginos and neutralinos in simplified models and on the parameters of the phenomenological Minimal Supersymmetric Standard Model. In simplified models, chargino masses are excluded up to 580 GeV in the presence of light sleptons and in the range 150–300 GeV in case of heavy sleptons for a massless lightest neutralino, significantly extending previous results.

ATLAS-CONF-2012-154
12 November 2012

1 Introduction

Supersymmetry (SUSY) [1–9] postulates the existence of SUSY particles, or "sparticles", with spin differing by one-half unit with respect to that of their Standard Model (SM) partner. If R-parity [10–14] is conserved, the lightest SUSY particle (LSP) is stable and sparticles can only be pair-produced and decay into final states with SM particles and LSPs. Charginos ($\tilde{\chi}_i^{\pm}$, $i = 1, 2$) and neutralinos ($\tilde{\chi}_j^0$, $j = 1, 2, 3, 4$) are the mass eigenstates formed from the linear superposition of the SUSY partners of the Higgs and electroweak gauge bosons. These are the Higgsinos, and the winos, zino, and bino, collectively known as gauginos. Naturalness requires the lightest $\tilde{\chi}_i^{\pm}$ and $\tilde{\chi}_j^0$ (and third-generation squarks) to have masses in the hundreds of GeV range [15, 16]. In scenarios where squark and gluino masses are larger than a few TeV, the direct production of gauginos may be the dominant SUSY process at the Large Hadron Collider (LHC). Charginos can decay into leptonic final states via sneutrinos ($\tilde{\nu}\ell$), sleptons ($\tilde{\ell}\nu$) or W bosons ($W\tilde{\chi}_1^0$), while unstable neutralinos can decay via sleptons ($\ell\tilde{\ell}$) or Z bosons ($Z\tilde{\chi}_1^0$).

This note presents a search with the ATLAS detector for the direct production of charginos and neutralinos decaying to a final state with three leptons (electrons or muons) and missing transverse momentum, the latter originating from the two undetected LSPs and the neutrinos. The analysis is based on $13.0\,\text{fb}^{-1}$ of proton-proton collision data delivered by the LHC at a centre-of-mass energy $\sqrt{s} = 8\,\text{TeV}$. No excess above the Standard Model expectation is observed and the results significantly extend the current mass limits on charginos and neutralinos set by ATLAS [17–19] and CMS [20]. Similar searches have been conducted at the Tevatron [21, 22] and LEP [23], where a model-independent lower limit of 103.5 GeV was set at 95% confidence level (CL) on the mass of promptly decaying charginos.

2 Detector Description

ATLAS [24] is a multipurpose particle detector with forward-backward symmetric cylindrical geometry. It includes an inner tracker (ID) immersed in a 2 T magnetic field providing precision tracking of charged particles for pseudorapidities[1] $|\eta| < 2.5$. Calorimeter systems with either liquid argon or scintillating tiles as the active media provide energy measurements over the range $|\eta| < 4.9$. The muon detectors are positioned outside the calorimeters and are contained in a toroidal magnetic field produced by air-core superconducting magnets with field integrals varying from 1 T·m to 8 T·m. They provide trigger and high-precision tracking capabilities for $|\eta| < 2.4$ and $|\eta| < 2.7$, respectively.

3 New Physics Scenarios

In this analysis, results are interpreted in the phenomenological Minimal Supersymmetric SM (pMSSM [25]) and in simplified models [26].

In the pMSSM the mixings for the $\tilde{\chi}_i^{\pm}$ and $\tilde{\chi}_j^0$ depend on the gaugino masses M_1 and M_2, the Higgs mass parameter μ, and $\tan\beta$, the ratio of the vacuum expectation values of the two Higgs doublets. The dominant mode for gaugino production leading to three-lepton final states is $\tilde{\chi}_1^{\pm}\tilde{\chi}_2^0$ production via the s-channel exchange of a virtual gauge boson. Other $\tilde{\chi}_i^{\pm}\tilde{\chi}_j^0$ processes contribute a maximum of 20% to three-lepton final states depending on the values of the mass parameters. The right-handed sleptons (including third-generation sleptons) are assumed to be degenerate and have a mass $m_{\tilde{\ell}_R} = (m_{\tilde{\chi}_2^0} + m_{\tilde{\chi}_1^0})/2$, set via the right-handed SUSY-breaking slepton mass parameter at the electroweak scale. In these scenarios, decays

[1] ATLAS uses a right-handed coordinate system with its origin at the nominal interaction point (IP) in the centre of the detector and the z-axis along the beam pipe. The x-axis points from the IP to the centre of the LHC ring, and the y-axis points upward. Cylindrical coordinates (r, ϕ) are used in the transverse plane, ϕ being the azimuthal angle around the beam pipe. The pseudorapidity is defined in terms of the polar angle θ as $\eta = -\ln\tan(\theta/2)$.

to sleptons are favoured. The parameter $\tan\beta$ is set to 6, yielding comparable branching ratios into each slepton generation. The masses of the gluinos, squarks and left-handed sleptons are chosen to be larger than 2 TeV. In order to achieve a Higgs mass close to 125 GeV [27], maximum mixing in the top squark sector is chosen by setting the corresponding trilinear couplings to $\sqrt{6}$, while all other trilinear couplings are set to zero.

In the simplified models considered, the masses and the decay modes of the relevant particles ($\tilde{\chi}_1^{\pm}$, $\tilde{\chi}_2^0$, $\tilde{\chi}_1^0$, $\tilde{\nu}$, $\tilde{\ell}_{\mathrm{L}}$) are the only free parameters. The $\tilde{\chi}_2^0$ and $\tilde{\chi}_1^{\pm}$ are set to be wino-like and mass degenerate, and the $\tilde{\chi}_1^0$ is set to be bino-like. Two different scenarios for the associated production of $\tilde{\chi}_1^{\pm}$ and $\tilde{\chi}_2^0$ are considered. In the first case, the $\tilde{\chi}_1^{\pm}$ and $\tilde{\chi}_2^0$ decay with a branching fraction of 1/6 through $\tilde{e}_L$, $\tilde{\mu}_L$, $\tilde{\tau}_L$, $\tilde{\nu}_e$, $\tilde{\nu}_\mu$, and $\tilde{\nu}_\tau$ with mass $m_{\tilde{\nu}} = m_{\tilde{\ell}_L} = (m_{\tilde{\chi}_1^0} + m_{\tilde{\chi}_1^{\pm}})/2$. In the second scenario, the $\tilde{\chi}_1^{\pm}$ and $\tilde{\chi}_2^0$ decay via W and Z bosons that may be off-mass-shell. In the simplified models, the branching ratios for decays via the Higgs bosons are set to zero.

4 Monte Carlo simulation

Several Monte Carlo (MC) generators are used to simulate SM processes and new physics signals relevant for this analysis. SHERPA [28] is used to simulate the diboson processes WW, WZ and ZZ, where "Z" also includes virtual photons. These diboson samples correspond to all SM diboson diagrams leading to the $\ell\nu\ell'\nu'$, $\ell\ell\ell'\nu'$, and $\ell\ell\ell'\ell'$ final states, where $\ell, \ell' = e, \mu, \tau$ and $\nu, \nu' = \nu_e, \nu_\mu, \nu_\tau$. Interference between the diagrams is taken into account. MadGraph [29] is used for the $t\bar{t}W$, $t\bar{t}WW$, $t\bar{t}Z$, $W\gamma$ and $Z\gamma$ processes. The "triboson" processes, WWW, ZWW and ZZZ are also simulated using MadGraph. POWHEG [30] is chosen for the simulation of the pair production of top quarks, MC@NLO [31] and ACERMC [32] are used for the simulation of single top production, and ALPGEN [33] is used to simulate W+jets and Z+jets processes. Expected diboson yields are normalised using next-to-leading-order (NLO) QCD predictions obtained with MCFM [34, 35]. Triboson contributions are normalised to NLO predictions [36]. The top-quark pair-production contribution is normalised to approximate next-to-next-to-leading-order calculations (NNLO) [37] and the $t\bar{t}W$, $t\bar{t}WW$, $t\bar{t}Z$ contributions are normalised to NLO predictions [38,39]. The QCD NNLO cross-sections from the FEWZ program [40, 41] are used for normalisation of the inclusive W+jets and Z+jets processes.

The choice of the parton distribution functions (PDFs) depends on the generator. The CTEQ6L1 [42] PDFs are used with MadGraph and ALPGEN, and the CT10 [43] PDFs with POWHEG, MC@NLO and SHERPA.

Fragmentation and hadronisation for the ALPGEN and MC@NLO samples are performed with HERWIG, while for MadGraph, PYTHIA [44] is used, and for SHERPA these are performed internally. JIMMY [45] is interfaced to HERWIG for simulation of the underlying event. For all MC samples, the propagation of particles through the ATLAS detector is modelled using GEANT4 [46] using the full ATLAS detector simulation [47] (except the $t\bar{t}$ POWHEG sample which uses fast detector simulation AtlFast-II). The effect of multiple proton-proton collisions from the same or different bunch crossings is incorporated into the simulation by overlaying additional minimum-bias events generated by PYTHIA onto hard-scatter events. Simulated events are weighted to match the distribution of the number of interactions per bunch crossing observed in data. Simulated data are reconstructed in the same manner as the data.

5 Event Reconstruction and Preselection

The data sample was collected with an inclusive selection of double-lepton triggers, where at least two reconstructed leptons are required to have triggered the event, with transverse energy or momentum above threshold. For dimuon triggers, the two muons are each required to have $p_{\mathrm{T}}^{\mu} > 14$ GeV (or one having $p_{\mathrm{T}}^{\mu} > 18$ GeV and the other $p_{\mathrm{T}}^{\mu} > 8$ GeV). For dielectron triggers, the two electrons are each required

to have $E_{\mathrm{T}}^{e} > 14\,\mathrm{GeV}$ (or one having $E_{\mathrm{T}}^{e} > 25\,\mathrm{GeV}$ and the other $E_{\mathrm{T}}^{e} > 10\,\mathrm{GeV}$). Thresholds for electron-muon triggers are $E_{\mathrm{T}}^{e} > 14\,\mathrm{GeV}$ and $p_{\mathrm{T}}^{\mu} > 8\,\mathrm{GeV}$, or $E_{\mathrm{T}}^{e} > 10\,\mathrm{GeV}$ and $p_{\mathrm{T}}^{\mu} > 18\,\mathrm{GeV}$. These thresholds are chosen such that the overall fiducial trigger efficiency is high, typically in excess of 90%, and independent of the transverse momentum of the triggerable objects within uncertainties. MC simulated events are accepted if the outcome of the trigger simulation satisfies the above requirements.

Events recorded during normal running conditions are analysed if the primary vertex has five or more tracks associated to it. The primary vertex of an event is identified as the vertex with the highest $\Sigma p_{\mathrm{T}}^{2}$ of associated tracks.

Electrons must satisfy "medium" identification criteria [48] and fulfil $E_{\mathrm{T}} > 10\,\mathrm{GeV}$ and $|\eta| < 2.47$, where E_{T} and η are determined from the calibrated clustered energy deposits in the electromagnetic calorimeter and the matched ID track, respectively. Muons are reconstructed by combining tracks in the ID and tracks in the muon spectrometer [49]. Reconstructed muons are considered as candidates if they have transverse momentum $p_{\mathrm{T}} > 10\,\mathrm{GeV}$ and $|\eta| < 2.4$.

Jets are reconstructed with the anti-k_t algorithm [50] with a radius parameter of $R = 0.4$ using topological clusters. The clusters are calibrated using local cluster calibration, consisting of weighting differently the energy deposits arising from electromagnetic showers and those from hadronic showers. The final jet energy calibration includes the jet energy scale, which corrects the calorimeter response to the true jet energy. The correction factors were obtained from simulation and have been refined and validated using data. Jets considered in this analysis have $E_{\mathrm{T}} > 20\,\mathrm{GeV}$ and $|\eta| < 2.5$. The p_{T}-weighted fraction of the tracks in the jet that are associated with the primary vertex is required to be larger than 0.5.

Events containing jets failing the quality criteria described in Ref. [51] are rejected to suppress both SM and beam-induced backgrounds. Jets are identified as containing b-hadron decays, and thus called "b-tagged", using a multivariate technique based on quantities such as the impact parameters of the tracks associated to a reconstructed secondary vertex. The chosen working point of the b-tagging algorithm [52] correctly identifies b-quark jets in simulated top-quark decays with an efficiency of 85% and with a light-flavour jet misidentification rate of about 10% for jets with $E_{\mathrm{T}} > 20\,\mathrm{GeV}$ and $|\eta| < 2.5$ [53].

The missing transverse momentum, $E_{\mathrm{T}}^{\mathrm{miss}}$, is the magnitude of the vector sum of the transverse momentum or transverse energy of all $p_{\mathrm{T}} > 10\,\mathrm{GeV}$ muons, $E_{\mathrm{T}} > 10\,\mathrm{GeV}$ electrons, $E_{\mathrm{T}} > 20\,\mathrm{GeV}$ jets, and calibrated calorimeter energy clusters with $|\eta| < 4.9$ not associated to these objects. Reconstructed tracks are used to suppress pileup in the soft components of the $E_{\mathrm{T}}^{\mathrm{miss}}$ [54].

In this analysis, "tagged" leptons are leptons separated from each other and from candidate jets as described below. If two candidate electrons are reconstructed with $\Delta R \equiv \sqrt{(\Delta\phi)^2 + (\Delta\eta)^2} < 0.1$, the lower energy one is discarded. Candidate jets within $\Delta R = 0.2$ of an electron candidate are rejected. To suppress leptons originating from semi-leptonic decays of c- and b-quarks, all lepton candidates are required to be separated from candidate jets by $\Delta R > 0.4$. Muons undergoing bremsstrahlung can be reconstructed with an overlapping electron candidate. To reject these, tagged electrons and muons separated from jets and reconstructed within $\Delta R = 0.1$ of each other are both discarded. Events containing one or more tagged muons that have transverse impact parameter with respect to the primary vertex $|d_0| > 0.2\,\mathrm{mm}$ or longitudinal impact parameter with respect to the primary vertex $|z_0| > 1\,\mathrm{mm}$ are rejected to suppress cosmic muon background.

"Signal" leptons are tagged leptons that are required to be isolated: the scalar sum of the transverse momenta of tracks within a cone of $\Delta R = 0.3$ around the lepton candidate, and excluding the lepton candidate track itself, must be less than 16% (12%) of the lepton E_{T} (p_{T}) for electrons (muons). Tracks selected for the electron (muon) isolation requirement defined above are those which have $p_{\mathrm{T}} > 0.4$ (1.0) GeV and are associated to the primary vertex of the event. To suppress leptons originating from secondary vertices, the distance of closest approach of the lepton track to the primary vertex normalised to its uncertainty is required to satisfy $|d_0|/\sigma(d_0) < 5\,(3)$ and $|z_0 \sin\theta| < 0.4\,(1)\,\mathrm{mm}$ for electrons (muons). Signal electrons must also pass "tight" identification criteria [48] and the sum of the energy deposits in

Table 1: The selection requirements for the three signal regions. All regions require exactly three signal leptons and a same-flavour opposite-sign (SFOS) lepton pair with mass $m_{\mathrm{SFOS}} > 12\,\mathrm{GeV}$. Events with $m_{\mathrm{SFOS}} < 12\,\mathrm{GeV}$ are rejected. The m_{T} is calculated from the $E_{\mathrm{T}}^{\mathrm{miss}}$ and the lepton not forming the SFOS lepton pair closest to the Z mass.

Selection	SR1a	SR1b	SR2
Targeted $\tilde{\chi}_2^0$ decay	$\tilde{l}^{(*)}$ or Z^*		on-shell Z
$\lvert m_{\mathrm{SFOS}} - m_Z \rvert$	$> 10\,\mathrm{GeV}$		$< 10\,\mathrm{GeV}$
Number of b-jets	0		any
$E_{\mathrm{T}}^{\mathrm{miss}}$	$> 75\,\mathrm{GeV}$		$> 120\,\mathrm{GeV}$
m_{T}	any	$> 110\,\mathrm{GeV}$	$> 110\,\mathrm{GeV}$
p_{T} of leptons	$> 10\,\mathrm{GeV}$	$> 30\,\mathrm{GeV}$	$> 10\,\mathrm{GeV}$

the calorimeter (corrected for pileup effects) within a cone of $\Delta R = 0.3$ around the electron candidate is required to be less than 18% of the electron E_{T}.

6 Signal Region Selection

Selected events must contain exactly three signal leptons. As R-parity conserving leptonic decays of $\tilde{\chi}_j^0$ yield same-flavour opposite-sign (SFOS) lepton pairs, the presence of at least one such pair is required. The invariant mass of any SFOS lepton pair must be above 12 GeV to suppress background from low-mass resonances and the missing transverse momentum must satisfy $E_{\mathrm{T}}^{\mathrm{miss}} > 75\,\mathrm{GeV}$.

Three signal regions are then defined: two "Z-depleted" regions (SR1a and SR1b), with no SFOS pairs having invariant mass within 10 GeV of the nominal Z-boson mass; and a "Z-enriched" one (SR2), where at least one SFOS pair has an invariant mass within 10 GeV of the Z-boson mass. Events in SR1a and SR1b are further required to contain no b-tagged jets to suppress contributions from b-jet-rich background processes, where a lepton could originate from the decay of a heavy-flavor quark. SR1b is designed to increase sensitivity to scenarios characterised by large mass splittings between the heavy gauginos and the LSP by requiring all three leptons to have $p_{\mathrm{T}} > 30\,\mathrm{GeV}$. In both SR1b and SR2, the transverse mass variable $m_{\mathrm{T}} = \sqrt{2 \cdot E_{\mathrm{T}}^{\mathrm{miss}} \cdot p_{\mathrm{T}}^{\ell} \cdot (1 - \cos\Delta\phi_{\ell, E_{\mathrm{T}}^{\mathrm{miss}}})}$ must take values greater than 110 GeV, where the lepton entering the m_{T} calculation is the one not included in the lepton pair with invariant mass closest to the nominal Z-boson mass. The m_{T} requirement is introduced to suppress background from WZ events. In SR2, the $E_{\mathrm{T}}^{\mathrm{miss}}$ requirement is raised to 120 GeV to further suppress the WZ background. The SR1a/b regions target neutralino decays via intermediate sleptons or via off-shell Z bosons while SR2 targets decays via an on-shell Z boson with large $E_{\mathrm{T}}^{\mathrm{miss}}$. No signal region is defined addressing the scenarios with neutralino decaying via on-shell Z bosons with intermediate $E_{\mathrm{T}}^{\mathrm{miss}}$. There is no requirement on the number of non-b jets in any signal region. Table 1 summarises the selection requirements for the three signal regions.

7 Standard Model Background Estimation

Several SM processes contribute to the background in the signal regions. A background process is considered "irreducible" if it leads to events with three isolated leptons, referred to as "real" leptons below. A "reducible" process has at least one "fake" object, that is either a lepton from a semileptonic decay of a heavy-flavour quark, a lepton from misidentified light-flavour quark or gluon jet, referred to

as light-flavour, or an electron from an isolated photon conversion.

7.1 Reducible Background Processes

The reducible background includes single- and pair-production of top-quarks and WW or W/Z produced in association with jets or photons. The dominant component is the production of top quarks, followed by Z+jets. The reducible background is estimated using a "matrix method" similar to that described in Ref. [55] and has been previously used in Refs. [17] and [19].

In this implementation of the matrix method, the signal lepton with the highest p_{T} or E_{T} is taken to be real, which is a valid assumption in 99% of the cases, based on simulation. The number of observed events with one or two fakes is then extracted from a system of linear equations relating the number of events with two additional signal or tagged candidates to the number of events with two additional candidates that are either real or fake. The coefficients of the linear equations are functions of the real-lepton identification efficiencies and of the fake-object misidentification probabilities.

The real identification efficiencies are obtained from MC simulation in the region of interest and are scaled by correction factors to account for potential differences with respect to data. The real correction factors are obtained in a control region enriched in $Z \to \ell\ell$ decays and are found to be 0.99 ± 0.01 for both electrons and muons.

Misidentification probabilities for each relevant fake type (heavy flavour or conversion) and for each reducible background process, parameterised with the lepton p_{T} and η, are obtained using simulated events with one signal and two tagged leptons. These misidentification probabilities are then corrected using the ratio (fake correction factor) of the misidentification probability in data to that in simulation obtained from dedicated control samples. The fake correction factors are assumed to be independent of selected regions and any potential composition or kinematic differences. The validity of the assumption is confirmed by the agreement in the validation regions presented in Section 9. For heavy-flavour fakes, the correction factor is measured in a $b\bar{b}$-dominated control sample. This is defined by selecting events with only one b-tagged jet (containing a muon) and a tagged lepton, for which the fake rate is measured. Contaminating backgrounds that contain the production of real leptons from W decays include top-quark pair production and W bosons produced in association with a b-quark. An $E_{\mathrm{T}}^{\mathrm{miss}}$ requirement of less than 60 GeV suppresses both the $t\bar{t}$ and the W contamination, while requiring $m_{\mathrm{T}} < 50$ GeV reduces the W background. The remaining (~1% level) background is subtracted from data using MC predictions. The heavy flavour fake correction factor is found to be 0.73 ± 0.04 (0.84 ± 0.03) for electrons (muons). The correction factor for light-flavour fakes is measured in a Z + light-flavour jets dominated control sample. Events with two SFOS leptons and one tagged lepton of different flavour (i.e. $e^+e^- + \mu$ or $\mu^+\mu^- + e$) are selected and the invariant mass of the SFOS pair is required to lie within 10 GeV of the nominal Z-boson mass value. The three leptons in the event must be separated from all other leptons and jets in the event by $\Delta R > 0.4$ and events with b-tagged jets are rejected. To suppress leptons originating from conversions, the trilepton mass is required to lie outside 10 GeV of the nominal Z-boson mass value. Finally, $E_{\mathrm{T}}^{\mathrm{miss}} < 20$ GeV is required to suppress non-Z backgrounds. The light flavour fake correction factor is found to be 1.45 ± 0.26 (1.06 ± 0.22) for electrons (muons). The fake correction factor for the conversion candidates is determined in a sample of photons radiated from a muon in $Z \to \mu\mu$ decays. These are selected by requiring $m_{\mu\mu e}$ to lie within 10 GeV of the nominal Z-boson mass value. The conversion fake correction factor for electrons is found to be 1.03 ± 0.21. A weighted average misidentification probability is then calculated by weighting the corrected type- and process-dependent misidentification probabilities according to the relative contributions in a given signal or validation region, defined below.

7.2 Irreducible Background Processes

Irreducible processes include diboson (WZ and ZZ), triboson (WWW, ZZZ and ZWW) and $t\bar{t}W/Z$ production. The gauge bosons in the irreducible processes may be off-mass-shell. The ZZ, triboson, and $t\bar{t}W/Z$ contributions are determined using the corresponding MC samples, for which lepton and jet selection efficiencies are corrected to account for differences with respect to data.

The largest irreducible background, WZ, is determined using a semi-data-driven approach. The WZ background is fit to data in a control region including events with exactly three leptons with $p_{\mathrm{T}} > 20\,\mathrm{GeV}$, one SFOS lepton pair, a Z candidate, $50 < E_{\mathrm{T}}^{\mathrm{miss}} < 75\,\mathrm{GeV}$, a b-veto, and $50 < m_{\mathrm{T}} < 110\,\mathrm{GeV}$. The WZ purity in the control region is ~95%. Non-WZ backgrounds, both irreducible and reducible, are determined based on simulation or by using the matrix method and subtracted. A WZ normalisation factor, including statistical and systematic uncertainties as discussed in Section 8, of 1.03±0.14 with respect to the MC prediction is obtained in the control region under a background-only hypothesis and used to normalise the MC prediction of the WZ background in the validation regions. The $E_{\mathrm{T}}^{\mathrm{miss}}$ and m_{T} distributions in the WZ normalisation region are shown in Figure 1. To obtain the model-independent 95% CL upper limit on the new phenomena cross-section, a fit is performed simultaneously in the WZ control region and in the signal region, with floating WZ normalisation factor and a non-negative signal in the signal region only. This allows the propagation of the uncertainties on the normalisation factor. When setting limits on specific new physics scenarios, the signal contamination in the WZ control region is accounted for in the simultaneous fit.

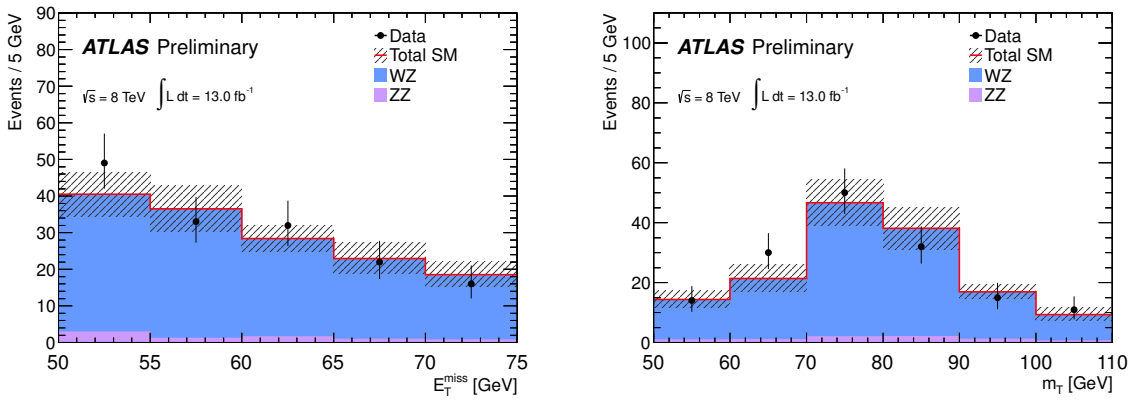

(a) (b)

Figure 1: For events in the WZ normalisation region, the (a) $E_{\mathrm{T}}^{\mathrm{miss}}$ and (b) m_{T} distributions are shown. The WZ component has been normalised to the data. The uncertainty band includes both statistical and systematic uncertainty, while the uncertainties on the data points are statistical only.

8 Systematic uncertainties

Several sources of systematic uncertainty are considered in the signal, control and validation regions. The systematic uncertainties affecting the simulation-based estimates (the yield of the irreducible background, the cross-section weighted misidentification probabilities, the signal yield) include the theoretical cross-section uncertainties due to renormalisation and factorisation scale and PDFs, the acceptance uncertainty due to PDFs and the choice of the MC generator, the uncertainty on the luminosity, the uncertainty due to the jet energy scale, jet energy resolution, lepton energy scale, lepton energy resolution, lepton efficiency, and the uncertainty due to b-tagging efficiency and mistag probability. The theoretical

cross-section uncertainties for the non-WZ irreducible backgrounds used in this analysis are 30%(50%) for $t\bar{t}W^{(*)}(Z^{(*)}, WW)$ [38, 39], 5% for ZZ [56] and a conservative 100% for tribosons. In SR1a, the total uncertainty on the irreducible background is 12%. This is dominated by the uncertainty on the cross-sections and the jet energy scale (6% each), followed by uncertainties on the electron efficiency and b-tagging efficiency and mistag probability (5% each). All the remaining uncertainties on the irreducible background in this signal region range between 0.1 and 5%. The total uncertainty on the irreducible background in SR1b is larger, at 40%. This is dominated by the 100% uncertainty on the triboson cross-section and also the residual uncertainty on the WZ acceptance due to the choice of MC generator, determined by comparing the SHERPA and POWHEG estimates. In SR2, the uncertainty on the irreducible background is 18%, with leading contributions from the generator uncertainty on the WZ contribution and those from the limited number of simulated events.

The uncertainty on the reducible background includes the MC uncertainty on the weights for the misidentification probabilities from the sources listed above (up to 10%) and the uncertainty due to the dependence of the misidentification probability on $E_{\mathrm{T}}^{\mathrm{miss}}$ (0.5–15%). Also included in the uncertainty on the reducible background is the uncertainty on the fake correction factors (4-21%). In SR1a, the uncertainty on the reducible background is dominated by the uncertainty due to the dependence of the misidentification probability on $E_{\mathrm{T}}^{\mathrm{miss}}$ at ~60% (~20% in SR1b and 0.02 events in SR2). In SR1b, the uncertainty on the reducible background is dominated by the statistical uncertainty from the limited number of data events with three tagged leptons, of which at least one is a signal lepton, at ~40% (10% in SR1a and 0.06 events in SR2). A systematic uncertainty is applied to the reducible background to account for a potential bias in the method as obtained from MC-based closure tests. The bias is negligible compared to the uncertainties from all other sources in SR1a and SR1b, but dominant in SR2 where it amounts to an uncertainty of 1.6 events on the reducible background of ~0.01 events. The estimate of the bias is limited by the available statistics of the MC samples in which the closure-test has been performed.

The total uncertainties on the signal yields are 20–40% and are calculated using the method described in Ref. [57], with the largest contribution from the uncertainty on the cross-sections. Signal cross-sections are calculated to NLO in the strong coupling constant using PROSPINO2 [58].

In all of the above, the value used for the uncertainty on the luminosity is 3.6%, measured using a technique similar to that of [59, 60]. A 5% uncertainty is applied to MC samples to describe differences in efficiency seen between the trigger in data and the MC trigger simulation. Correlations of systematic uncertainties between processes and regions are taken into account.

9 Background Model Validation

The background predictions have been tested in various validation regions. A region (VR1) dominated by Z^* and WZ^* production is selected by requiring three signal leptons, at least one SFOS lepton pair, $30\,\mathrm{GeV} < E_{\mathrm{T}}^{\mathrm{miss}} < 75\,\mathrm{GeV}$, and an on-shell Z-boson veto. A reducible-background dominated region (VR2, where top-quark pair-production and decay to two real and one fake lepton is the main contribution) is built by requiring three signal leptons, $E_{\mathrm{T}}^{\mathrm{miss}} > 50\,\mathrm{GeV}$ and by vetoing SFOS lepton pairs. Finally, a WZ-dominated region (VR3) is defined by selecting events with three signal leptons, at least one SFOS lepton pair, a Z candidate, and $30\,\mathrm{GeV} < E_{\mathrm{T}}^{\mathrm{miss}} < 50\,\mathrm{GeV}$. The selection requirements are summarised in Table 2. The data and SM expectation are in agreement within statistical and systematic uncertainties as shown in Table 3. The $E_{\mathrm{T}}^{\mathrm{miss}}$, m_{T} and m_{SFOS} distributions in VR1 are shown in Figure 2, while the $E_{\mathrm{T}}^{\mathrm{miss}}$ and b-jet multiplicity in VR2 are shown in Figure 3 and the $E_{\mathrm{T}}^{\mathrm{miss}}$ and m_{T} distributions in VR3 are shown in Figure 4.

Table 2: The selection requirements for the three validation regions. All regions require exactly three signal leptons and veto events with a same-flavour opposite-sign (SFOS) lepton pair with mass $m_{\mathrm{SFOS}} < 12\,\mathrm{GeV}$.

Selection	VR1	VR2	VR3
$\lvert m_{\mathrm{SFOS}} - m_Z \rvert$	$> 10\,\mathrm{GeV}$	SFOS veto	$< 10\,\mathrm{GeV}$
$E_{\mathrm{T}}^{\mathrm{miss}}$ min	30 GeV	50 GeV	30 GeV
$E_{\mathrm{T}}^{\mathrm{miss}}$ max	75 GeV	–	50 GeV

Table 3: Expected numbers of events from SM backgrounds and observed numbers of events in data, for $13.0\,\mathrm{fb}^{-1}$, in validation regions VR1, VR2 and VR3. The yields for two of the simplified model scenarios, "SUSY Ref. Point 1" with intermediate sleptons, ($m_{\tilde{\chi}_1^\pm}, m_{\tilde{\chi}_2^0}, m_{\tilde{\ell}_L}, m_{\tilde{\chi}_1^0} = 500, 500, 250, 0\,\mathrm{GeV}$) and "SUSY Ref. Point 2" with no intermediate sleptons, ($m_{\tilde{\chi}_1^\pm}, m_{\tilde{\chi}_2^0}, m_{\tilde{\chi}_1^0} = 250, 250, 0\,\mathrm{GeV}$) are also presented. Both statistical and systematic uncertainties are included.

Selection	VR1	VR2	VR3
$t\bar{t}$+V	3.1 ± 1.2	2.5 ± 0.8	3.9 ± 1.9
triboson	4 ± 4	2.1 ± 2.1	0.7 ± 0.7
ZZ	64 ± 17	0.41 ± 0.23	49 ± 4
WZ (normalised)	161 ± 19	4.5 ± 0.7	385 ± 50
Reducible Bkg.	121 ± 50	27 ± 13	185 ± 70
Total Bkg.	353 ± 60	36 ± 14	624 ± 90
Data	391	36	692
SUSY Ref. Point 1	1.2 ± 0.1	0.2 ± 0.0	0.0 ± 0.0
SUSY Ref. Point 2	0.3 ± 0.1	0.1 ± 0.0	1.5 ± 0.2

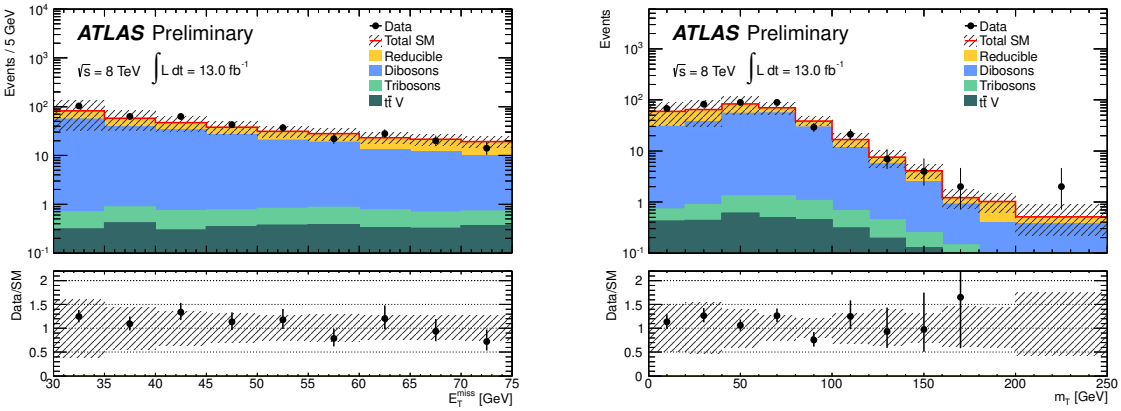

(a) (b)

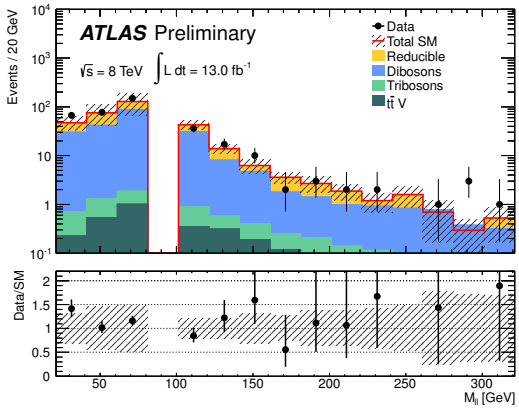

(c)

Figure 2: For events in VR1, the (a) $E_{\mathrm{T}}^{\mathrm{miss}}$, (b) m_{T} and (c) m_{SFOS} distributions are shown. The uncertainty band includes both statistical and systematic uncertainty, while the uncertainties on the data points are statistical only.

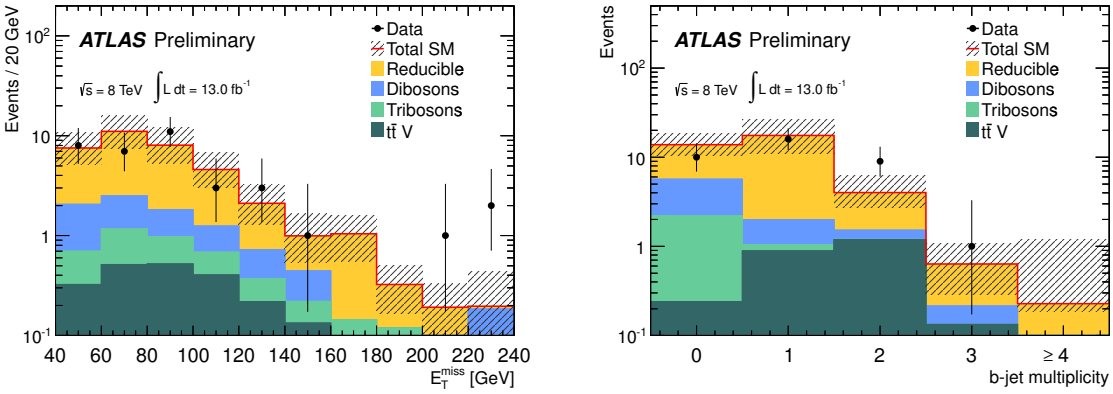

(a) (b)

Figure 3: For events in VR2, the (a) $E_{\mathrm{T}}^{\mathrm{miss}}$ and (b) b-jet multiplicity distributions are shown. The uncertainty band includes both statistical and systematic uncertainty, while the uncertainties on the data points are statistical only.

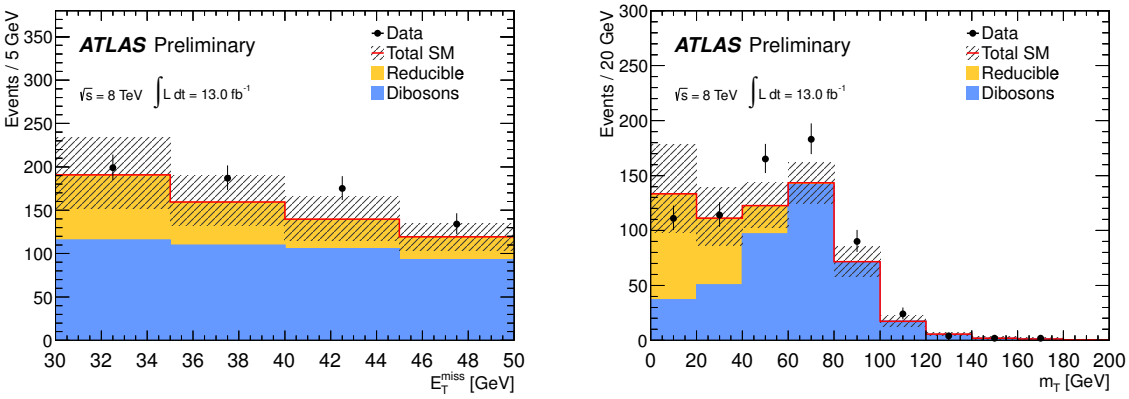

(a) (b)

Figure 4: For events in VR3, the (a) $E_{\mathrm{T}}^{\mathrm{miss}}$ and (b) m_{T} distributions are shown. The uncertainty band includes both statistical and systematic uncertainty, while the uncertainties on the data points are statistical only.

10 Results and Interpretation

The numbers of observed events and the prediction for SM backgrounds in SR1a, SR1b and SR2 are given in Table 4. Distributions of the $E_{\mathrm{T}}^{\mathrm{miss}}$ in SR1a, SR1b, and SR2 are presented in Figure 5.

Table 4: Expected numbers of events from SM backgrounds and observed numbers of events in data, for 13.0 fb^{-1}, in signal regions SR1a, SR1b and SR2. The yields for two of the simplified model scenarios, "SUSY Ref. Point 1" with intermediate sleptons, ($m_{\tilde{\chi}_1^\pm}, m_{\tilde{\chi}_2^0}, m_{\tilde{\ell}_L}, m_{\tilde{\chi}_1^0} = 500,\ 500,\ 250,\ 0$ GeV) and "SUSY Ref. Point 2" with no intermediate sleptons, ($m_{\tilde{\chi}_1^\pm}, m_{\tilde{\chi}_2^0}, m_{\tilde{\chi}_1^0} = 250,\ 250,\ 0$ GeV) are also presented. Both statistical and systematic uncertainties are included. Upper limits on the observed and expected visible production cross-section at 95% CL are also shown.

Selection	SR1a	SR1b	SR2
$t\bar{t}$+V	0.62 ± 0.28	0.13 ± 0.07	0.9 ± 0.4
triboson	3.0 ± 3.0	0.7 ± 0.7	0.34 ± 0.34
ZZ	2.0 ± 0.7	0.30 ± 0.23	0.10 ± 0.10
WZ (normalised)	34 ± 4	1.2 ± 0.6	4.7 ± 0.8
Reducible Bkg.	10 ± 6	0.8 ± 0.4	$0.012^{+1.6}_{-0.012}$
Total Bkg.	50 ± 8	3.1 ± 1.0	$6.1^{+2.0}_{-1.2}$
Data	48	4	4
SUSY Ref. Point 1	13.9 ± 1.0	11.4 ± 0.9	0.5 ± 0.1
SUSY Ref. Point 2	0.9 ± 0.1	0.3 ± 0.1	8.0 ± 0.6
Visible σ (exp)	< 1.5 fb	< 0.4 fb	< 0.5 fb
Visible σ (obs)	< 1.3 fb	< 0.5 fb	< 0.4 fb

No significant excess of events is found in any of the three signal regions. Upper limits on the visible cross-section, defined as the production cross-section times acceptance times efficiency, of 1.3 fb in SR1a, 0.5 fb in SR1b and 0.4 fb in SR2 are placed at 95% CL with the modified frequentist CL_s prescription [61]. All systematic uncertainties and their correlations are taken into account via nuisance parameters in a profile likelihood fit [62]. The corresponding expected limits are 1.5 fb, 0.4 fb and 0.5 fb, respectively.

SR1a and SR1b provide the best sensitivity for the pMSSM scenarios; in particular SR1a (SR1b) targets scenarios with small (large) mass splitting between the heavy gauginos and the LSP. The limits are calculated using the signal region providing the best expected limit for each of the model points. The uncertainties on the signal cross-section are not included in the limit calculation but their impact on the observed limit is indicated by the red-dotted lines.

The main features in the exclusion limits shown in Figure 6 as a function of the three parameters M_1 , M_2 and μ can be explained in broad terms as follows. For a given value of M_1 , for example M_1 = 100 GeV in Figure 6(a), the production cross-section decreases as M_2 and μ increase, which explains why limits become less stringent when both M_2 and μ take high values. In general, the sensitivity is reduced in the region at low M_2 and high μ, due to the small mass splitting between the $\tilde{\chi}_2^0$ and the $\tilde{\chi}_1^0$. When μ is greater than M_1 and M_2 , which is true for example in the rightmost part of the exclusion plots for $M_1 = 100$ GeV (Figure 6(a)) and $M_1 = 140$ GeV (Figure 6(b)), the mass of the gauginos does not depend on μ and the sensitivity remains constant as a function of μ. For $M_1 = 250$ GeV, two areas of exclusion are seen; one at low M_2 and low μ where the cross-section is high and another at high M_2 and high μ, where mass splittings are large. The area between the two exclusion areas is not excluded due

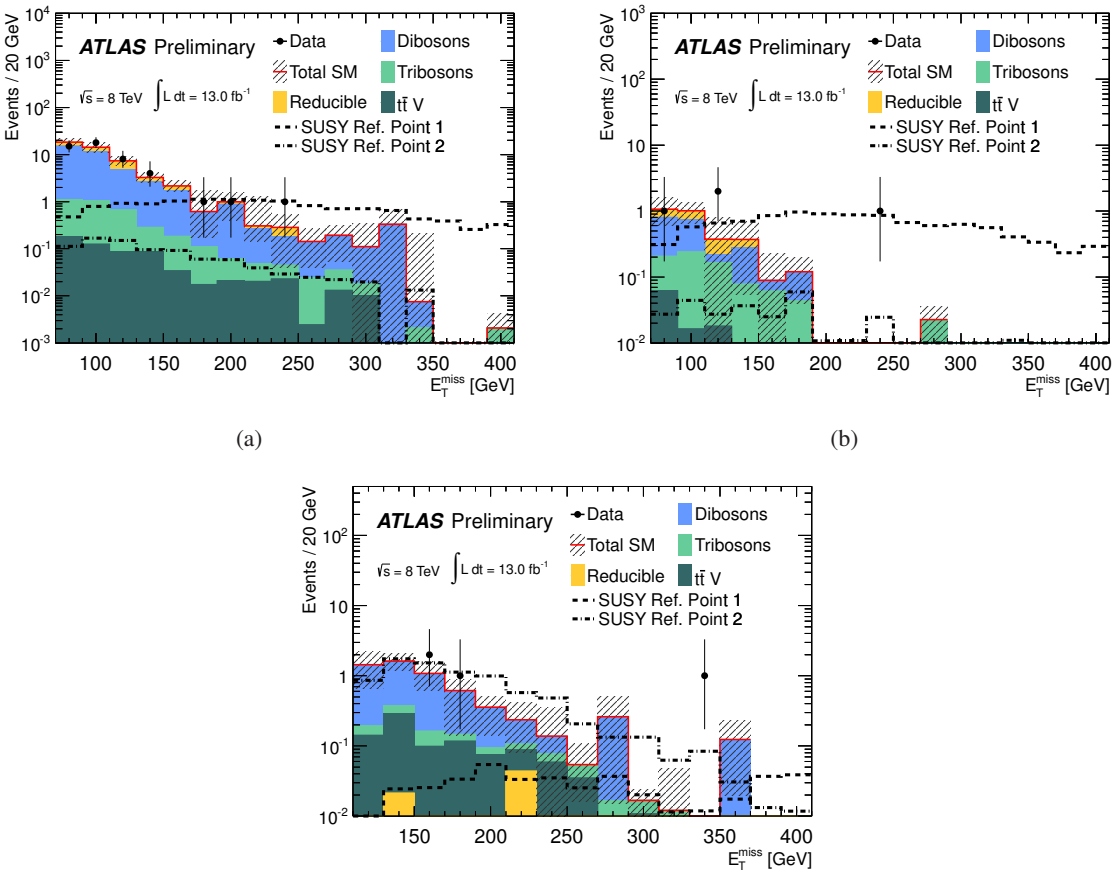

Figure 5: The $E_{\mathrm{T}}^{\mathrm{miss}}$ distributions for events in signal regions (a) SR1a, (b) SR1b and (c) SR2 are shown. The uncertainty band includes both statistical and systematic uncertainty, while the uncertainties on the data points are statistical only. The yields for two of the simplified model scenarios are also shown for illustration purposes: one with intermediate sleptons "SUSY Ref. Point 1" ($m_{\tilde{\chi}_1^\pm}, m_{\tilde{\chi}_2^0}, m_{\tilde{\ell}_L}, m_{\tilde{\chi}_1^0} = 500$, 500, 250, 0 GeV) and a second with no sleptons "SUSY Ref. Point 2" ($m_{\tilde{\chi}_1^\pm}, m_{\tilde{\chi}_2^0}, m_{\tilde{\chi}_1^0} = 250$, 250, 0 GeV). The signal distribution is not stacked on top of the expected background.

to low mass splittings between the $\tilde{\chi}_1^\pm$ and $\tilde{\chi}_1^0$. The value of $\tan\beta$ does not have a significant impact on $\sigma(pp \to \tilde{\chi}_i^\pm \tilde{\chi}_j^0) \times BR(\tilde{\chi}_i^\pm \tilde{\chi}_j^0 \to \ell\nu\tilde{\chi}_1^0 \ell\ell\tilde{\chi}_1^0)$, which decreases by 10% if $\tan\beta$ is raised from 6 to 10.

Region SR1b provides the best sensitivity to the simplified models with intermediate slepton decays for which the interpretation is shown in Figure 7(a). In these models, degenerate $\tilde{\chi}_1^\pm$ and $\tilde{\chi}_2^0$ masses up to 580 GeV are excluded for large mass differences from the $\tilde{\chi}_1^0$. Both SR1a and SR2 are used to interpret the results in the simplified model with gauginos decaying via gauge bosons for which the limits are shown in Figure 7(b). The signal region SR1a has the best sensitivity for small mass differences between the lightest neutralinos and is responsible for the exclusion area close to the diagonal. SR2 is sensitive to decays of $\tilde{\chi}_2^0$ into on-mass-shell Z bosons with high $E_{\mathrm{T}}^{\mathrm{miss}}$ and is responsible for the exclusion area far from the diagonal. The area between the two excluded regions requires a signal region sensitive to on-mass-shell Z boson decays with intermediate $E_{\mathrm{T}}^{\mathrm{miss}}$ values, which was not performed for this note.

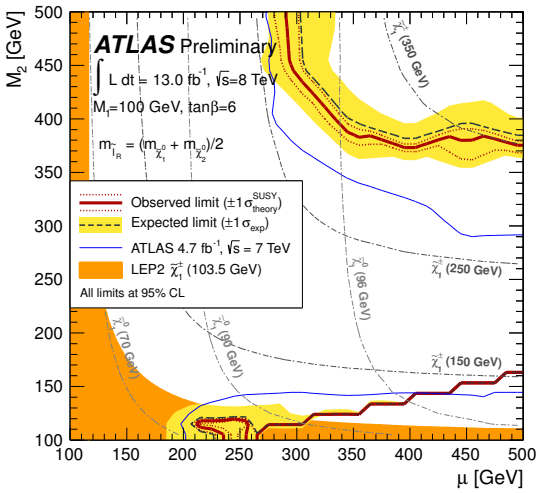

(a)

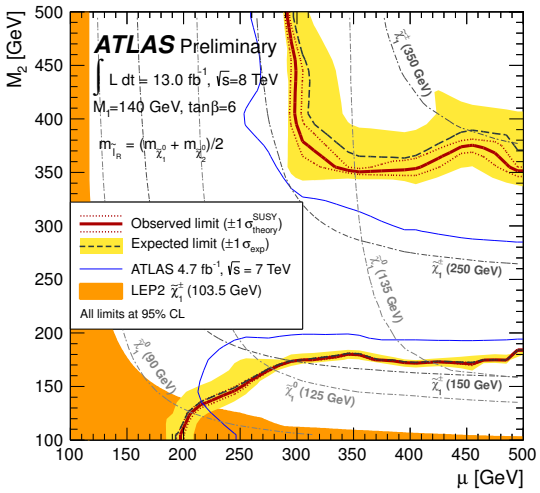

(b)

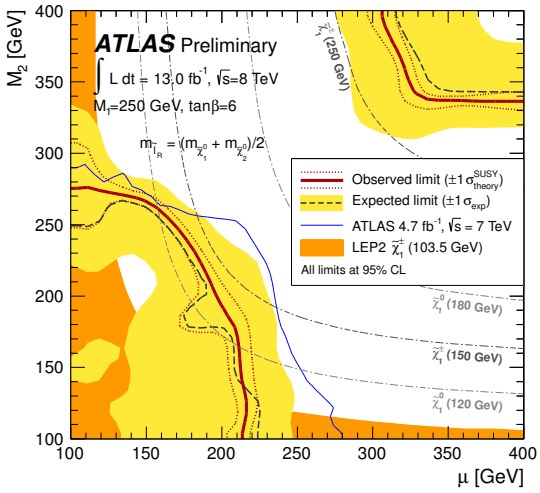

(c)

Figure 6: Observed and expected 95% CL limit contours for chargino and neutralino production in the pMSSM for (a) $M_1 = 100$ GeV, (b) $M_1 = 140$ GeV and (c) $M_1 = 250$ GeV, and light sleptons. The regions with low values of M_2 and μ are excluded for all values of M_1. In (c), high values of M_2 and μ are also excluded within the explored region. The expected and observed limits are calculated without signal cross-section uncertainty taken into account. The yellow band is the $\pm 1\sigma$ experimental uncertainty on the expected limit (black dashed line). The red dotted band is the $\pm 1\sigma$ signal theory uncertainty on the observed limit (red solid line). The blue lines correspond to the 7 TeV limits from the combination of the two lepton and three lepton analyses [17]. The LEP2 limit in the Figure corresponds to the limit on the $\tilde{\chi}_1^{\pm}$ mass in Ref. [63] as transposed to this pMSSM plane. Linear interpolation is used to account for the discrete nature of the signal grids. The exclusion contours are optimised by using in each signal grid point the CL values [61] from the most sensitive signal region (with the largest expected exclusion power).

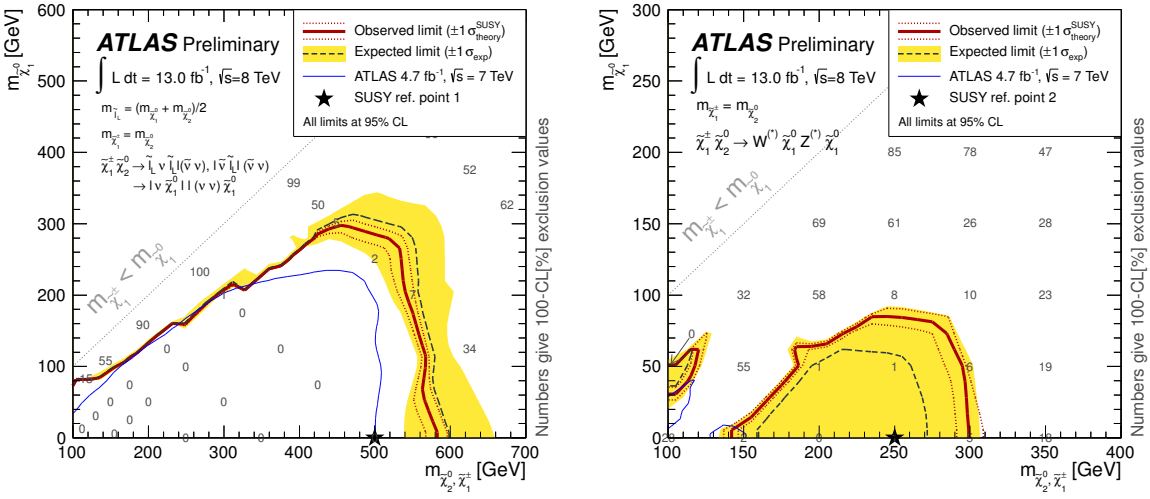

(a) (b)

Figure 7: Observed and expected 95% CL limit contours for chargino and neutralino production in the simplified model scenario with (a) intermediate slepton decay and (b) intermediate gauge boson decay. The 100−CL[%] value [61] is also shown for each of the simulated model points. The colour coding is the same as that in Figure 6. The blue lines correspond to the 7 TeV limits from the three lepton analysis [17].

11 Summary

Results from a search for direct production of charginos and neutralinos in the final state with three leptons (electrons or muons) and missing transverse momentum are reported. The analysis is based on 13.0 fb^{-1} of proton-proton collision data delivered by the LHC at $\sqrt{s}$ =8 TeV and collected by ATLAS. No significant excess of events is found in data above SM expectations. The null result is interpreted in the pMSSM and simplified models. For the simplified models with intermediate slepton decays, degenerate $\tilde{\chi}_1^{\pm}$ and $\tilde{\chi}_2^0$ masses up to 580 GeV are excluded for large mass differences with the $\tilde{\chi}_1^0$. For the simplified models with gauge boson decays, degenerate $\tilde{\chi}_1^{\pm}$ and $\tilde{\chi}_2^0$ masses up to 300 GeV are excluded for large mass differences with the $\tilde{\chi}_1^0$.

References

[1] H. Miyazawa, Prog. Theor. Phys. **36 (6)** (1966) 1266–1276.

[2] P. Ramond, Phys. Rev. **D 3** (1971) 2415–2418.

[3] Y. A. Gol'fand and E. P. Likhtman, JETP Lett. **13** (1971) 323–326.

[4] A. Neveu and J. H. Schwarz, Nucl. Phys. **B 31** (1971) 86–112.

[5] A. Neveu and J. H. Schwarz, Phys. Rev. **D 4** (1971) 1109–1111.

[6] J. Gervais and B. Sakita, Nucl. Phys. **B 34** (1971) 632–639.

[7] D. V. Volkov and V. P. Akulov, Phys. Lett. **B 46** (1973) 109–110.

[8] J. Wess and B. Zumino, Phys. Lett. **B 49** (1974) 52.

[9] J. Wess and B. Zumino, Nucl. Phys. **B 70** (1974) 39–50.

[10] P. Fayet, Phys. Lett. **B 64** (1976) 159.

[11] P. Fayet, Phys. Lett. **B 69** (1977) 489.

[12] G. R. Farrar and P. Fayet, Phys. Lett. **B 76** (1978) 575–579.

[13] P. Fayet, Phys. Lett. **B 84** (1979) 416.

[14] S. Dimopoulos and H. Georgi, Nucl. Phys. **B 193** (1981) 150.

[15] R. Barbieri and G. Giudice, Nucl. Phys. **B 306** (1988) 63.

[16] B. de Carlos and J. Casas, Phys. Lett. **B 309** (1993) 320–328, arXiv:hep-ph/9303291.

[17] ATLAS Collaboration, arXiv:1208.3144 [hep-ex].

[18] ATLAS Collaboration, arXiv:1208.2884 [hep-ex].

[19] ATLAS Collaboration, Phys. Rev. Lett. **108** (2012) 261804, arXiv:1204.5638 [hep-ex].

[20] CMS Collaboration, S. Chatrchyan et al., arXiv:1209.6620 [hep-ex].

[21] D0 Collaboration, V. Abazov et al., Phys. Lett. **B 680** (2009) 34–43, arXiv:0901.0646 [hep-ex].

[22] CDF Collaboration, T. Aaltonen et al., Phys. Rev. Lett. **101** (2008) 251801, arXiv:0808.2446 [hep-ex].

[23] LEPSUSYWG, ALEPH, DELPHI, L3, OPAL Collaborations, LEPSUSYWG/01-03.1 (2001). http://lepsusy.web.cern.ch/lepsusy/www/inos_moriond01/charginos_pub.html.

[24] ATLAS Collaboration, JINST **3** (2008) S08003.

[25] A. Djouadi et al., Comput. Phys. Commun. **176** (2007) 426–455, arXiv:hep-ph/0211331 [hep-ph].

[26] J. Alwall et al., Phys. Rev. **D 79** (2009) 075020, arXiv:0810.3921 [hep-ph].

[27] ATLAS Collaboration Collaboration, Phys.Lett. **B716** (2012) 1–29, arXiv:1207.7214 [hep-ex].

[28] T. Gleisberg et al., JHEP **0902** (2009) 007, arXiv:0811.4622 [hep-ph].

[29] J. Alwall et al., JHEP **09** (2007) 028, arXiv:0706.2334 [hep-ph].

[30] P. Nason, JHEP **0411** (2004) 040, arXiv:hep-ph/0409146.

[31] S. Frixione and B. R. Webber, arXiv:hep-ph/0601192.

[32] B. P. Kersevan and E. Richter-Was, Comput. Phys. Commun. **149** (2003) 142–194, arXiv:hep-ph/0201302 [hep-ph].

[33] M. L. Mangano et al., JHEP **0307** (2003) 001, arXiv:hep-ph/0206293.

[34] J. M. Campbell and R. K. Ellis, Phys. Rev. **D 60** (1999) 113006, arXiv:hep-ph/9905386 [hep-ph].

[35] J. M. Campbell, R. K. Ellis, and C. Williams, JHEP **1107** (2011) 018, arXiv:1105.0020 [hep-ph].

[36] F. Campanario et al., Phys. Rev. **D 78** (2008) 094012, arXiv:0809.0790 [hep-ph].

[37] M. Aliev et al., Comput. Phys. Commun. **182** (2011) 1034–1046, arXiv:1007.1327 [hep-ph].

[38] A. Kardos, Z. Trocsanyi, and C. Papadopoulos, Phys. Rev. **D 85** (2012) 054015, arXiv:1111.0610 [hep-ph].

[39] J. M. Campbell and R. K. Ellis, JHEP **1207** (2012) 052, arXiv:1204.5678 [hep-ph].

[40] K. Melnikov and F. Petriello, Phys. Rev. **D 74** (2006) 114017, arXiv:hep-ph/0609070 [hep-ph].

[41] C. Anastasiou et al., Phys. Rev. **D 69** (2004) 094008, arXiv:hep-ph/0312266 [hep-ph].

[42] P. M. Nadolsky et al., Phys. Rev. **D 78** (2008) 013004, arXiv:0802.0007 [hep-ph].

[43] H.-L. Lai et al., Phys. Rev. **D 82** (2010) 074024, arXiv:1007.2241 [hep-ph].

[44] T. Sjostrand, S. Mrenna, and P. Z. Skands, JHEP **0605** (2006) 026, arXiv:hep-ph/0603175 [hep-ph].

[45] J. Butterworth et al., Z. Phys. **C 72** (1996) 637–646, arXiv:hep-ph/9601371 [hep-ph].

[46] GEANT4 Collaboration, Nucl. Instrum. Meth. **A 506** (2003) 250–303.

[47] ATLAS Collaboration, Eur. Phys. J. **C 70** (2010) 823–874.

[48] ATLAS Collaboration, Eur. Phys. J. **C 72** (2012) 1909, arXiv:1110.3174 [hep-ex].

[49] ATLAS Collaboration, JHEP **1012** (2010) 060, arXiv:1010.2130 [hep-ex].

[50] M. Cacciari, G. P. Salam, and G. Soyez, JHEP **0804** (2008) 063, arXiv:0802.1189 [hep-ph].

[51] ATLAS Collaboration, arXiv:1112.6426 [hep-ex].

[52] ATLAS Collaboration, ATLAS-CONF-2011-102. http://cdsweb.cern.ch/record/1369219.

[53] ATLAS Collaboration, ATLAS-CONF-2012-043. http://cdsweb.cern.ch/record/1435197.

[54] ATLAS Collaboration, ATLAS-CONF-2012-101. http://cdsweb.cern.ch/record/1463915.

[55] ATLAS Collaboration, Eur. Phys. J. **C 71** (2011) 1577, arXiv:1012.1792 [hep-ex].

[56] ATLAS Collaboration, ATL-COM-PHYS-2010-695. http://cdsweb.cern.ch/record/1287902.

[57] M. Kramer et al., arXiv:1206.2892 [hep-ph].

[58] W. Beenakker et al., Nucl. Phys. **B 492** (1997) 51–103, arXiv:hep-ph/9610490.

[59] ATLAS Collaboration, Eur. Phys. J. **C 71** (2011) 1630, arXiv:1101.2185 [hep-ex].

[60] ATLAS Collaboration, ATLAS-CONF-2011-116. http://cdsweb.cern.ch/record/1376384.

[61] A. L. Read, J. Phys. G: Nucl. Part. Phys. **28** (2002) 2693.

[62] G. Cowan et al., EPJC **71** (2011) 1–19.

[63] K. Nakamura and Particle Data Group, J. Phys. G: Nucl. Part. Phys. **37** (2010) 075021.